Development of Compact MIMO Antennas with Enhanced Isolation and Diversity Parameters for Efficient 5GA Communication

Dr. Abdul Rahiman Sheik[1], B. Divya Naga Sowmya[2], G. Venkata Sai Teja [3],

G. Hari[4], Ch. Vijay Babu[5], B. Ram Unmeelya[6]

[1] Associate Professor, Dept of ECE, NRI Institute of Technology, Agiripalli, Andhra Pradesh

[2,3,4,5,6] Dept of ECE, NRI Institute of Technology, Agiripalli. Andhra Pradesh

Abstract: The deployment of 5G networks demands antenna systems that strike a balance between compactness, efficiency, and robust performance. This project presents a novel compact MIMO antenna design engineered to enhance isolation and diversity parameters, addressing key challenges in modern communication systems. By employing innovative isolation techniques such as electromagnetic bandgap (EBG) materials, and decoupling networks, the proposed design minimizes mutual coupling and improves signal integrity. Additionally, strategic element positioning and polarization diversity methods are integrated to optimize spatial multiplexing and reduce envelope correlation. The resulting antenna system not only ensures high gain and broad bandwidth but also maintains a minimal footprint, ideal for space-constrained 5G devices. Rigorous simulation and prototype testing validate its effectiveness, showcasing improved isolation, enhanced diversity performance, and superior communication reliability. The parametric study of the proposed antenna was carried out using the HFSS simulator.

Key Words: MIMO Antenna, Electromagnetic Bandgap (EBG), 5G Technology, HFSS Software.

1. INTRODUCTION

The wireless communications sector is recognized as one of the most advanced and rapidly evolving domains within the telecommunications industry. The capacity for data transmission faces increasing challenges as the demand for both personal and commercial applications surges. Consequently, the growing number of subscribers to the Radio Frequency (RF) spectrum and its applications has led to spectrum congestion. This issue impacts both signal transmission and reception systems. As the frequency of components increases, the size of the radiation elements decreases, and their wavelengths shorten. The current wireless communication system needs to fulfill society's requirements and improve the spectrum parameters.

5G, the latest generation, is currently being launched. It offers incredibly fast data speeds of up to 20 Gbps, which is 100 times the data transfer speed compared to 4G. This enables seamless use of virtual and augmented reality applications, ultra-high-resolution video streaming, and faster internet browsing. Key features of 5G include ultra-fast speeds, low latency, high capacity, and improved reliability, making it perfect for advanced applications like virtual reality and gaming. In the present generation, Fifth Generation New Radio (5G-NR) has emerged as a future technology in the areas of mobile communication, Internet of Things (IoT), auto machines, health care, and beyond.

5G technology requires enhanced speed, capacity, and spatial diversity while minimizing multi path fading. Researchers and designers are focused on improving these aspects to make 5G more effective for current and future needs. 5G technology classified 8 specifications, as shown in Fig. 1.3 based on 3GPP and International Telecommunications Union Radio communication Sector (ITR-U) for millimeter Wave frequencies, i.e., 30-300 GHz, it can operate both bands of lower (sub-6 GHz) and higher mm-Wave frequency bands. Next frequency band categories three frequency bands in the microwave spectrum: sub-1 GHz (below 1 GHz), FR-1 (1 GHz to 6 GHz), known as the sub-6 GHz band, and FR-2 (6 GHz to 30 GHz), known as the mm- wave frequency band. Figure 1.4 displays the frequency spectrum and corresponding bands, displaying specific ranges and bands.

5G technology significantly surpasses 4G in speed, delivering peak data rates up to 20 Gigabits per second (Gbps) and average rates exceeding 100 Mbps. The use of low-density parity-check (LDPC) codes for forward error correction ensures low latency. 5G also supports advanced techniques like Beam Division Multiple Access (BDMA) and Filter Bank Multi Carrier (FBMC), which enhance system capacity and spectral efficiency. BDMA manages multiple users efficiently, while FBMC improves spectral usage. Additionally, 5G's low latency enables real-time, high-quality video applications, especially when combined with AI for advanced video analytics. The technology supports data rates ranging from 2 to 20 Gbps, a connection density of one million devices per square kilometer, and exceptional connection reliability.

2. ANTENNA DESIGN METHODOLOGY

A. Single Monopole Antenna

The design intends to optimize the performance of the 2x1 configuration MIMO antenna system with a gap between the antennas (edge to edge) ranging from 13.5 mm to 15.5 mm or center-to-center gaps (G) varying from 31.5 mm to 33.5 mm. To create a more compact antenna with better diversity parameter results, a parametric study has to be done, and the "G" has to be optimized to 32.5mm. Further, a decoupling element is added between the antennas to reduce S21 and improve isolation in the scenario described. The decoupling element's optimized dimensions are d2 (1 mm) in width and d1 (17 mm) in length. It is shown in Figure 5.2(c). Moreover, a ground branch element is introduced and connected at the center of DGS, with a tuned length of d3 (23 mm) and a width of d4 (0.5 mm), affecting the decoupling performance. The parametric study covers a ground slot width (c) optimized at 3mm, which enhances bandwidth, reflection coefficient, and isolation. A thorough strategy is used for lowering mutual coupling and enhancing isolation in the 2x1 MIMO antenna.

The patch is mounted on a 1.6-mm-high chassis, situated on a Rogers RO3003 substrate with a dielectric constant of εr=3.2 (with a loss tangent of 0.0013). Ant.1 incorporates a partial ground, while Ant.2 incorporates a rectangular slot etched into the ground plane. Ant.3, on the other hand, features a T-shaped stub etched into the ground plane and printed on the bottom of the substrate. To further optimize the performance, we need to conduct a thorough investigation into the placement of the T shaped slot on the ground plane. This optimization ranges from 8mm to 9mm, with a specific value of g2 set at 8.5 mm. This T-shaped slot effectively functions as a DGS, altering the current distribution across the radiator. Consequently, it leads to an increased bandwidth and a reduction in the minimum 37 38 reflection coefficient, particularly at the resonance frequency of 3.52 GHz. The dimensional parameters of the designs are listed.

B. Proposed two port MIMO antenna design and Analysis

Below figures are illustrates a multi-antenna compact design. It has two MIMO (Multiple Input, Multiple Output) antenna ports and offers gradual improvements for better isolation. The proposed antenna shared a symmetrical common ground, the s11 and s21 are the same as s22 and s12, respectively. It includes a T-shaped parasitic element, grounded branches, and DGS, which significantly reduces mutual coupling between the two antennas and adds impedance. DGS illustrate the current distribution on the surface, The DGS supports in retrieving the current surface, adapting the rectangular slots etched into the ground, and enhancing the bandwidth and isolation of antenna adjustment.

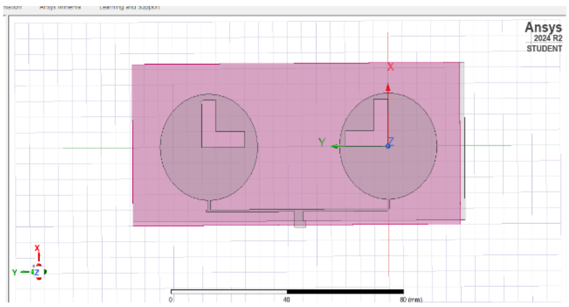

Fig.2.1 Top View of MIMO Antenna Structure Enclosed Within Radiation Boundary

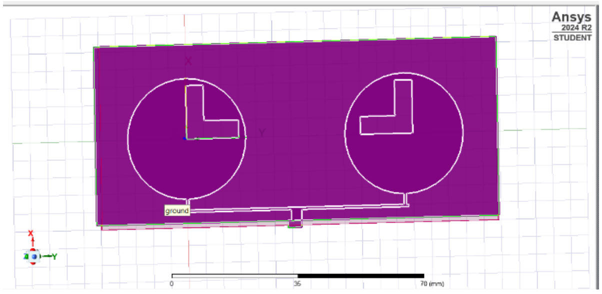

Fig.2.2. Top View of the Designed MIMO Antenna Geometry with Modified Circular Patch Elements in HFSS

The gap or slots are etched from the ground plane to achieve isolation from changes in current distribution in Fig.4. The mutual coupling is further reduced by loading two vertically grounded branches, which also enhances impedance matching and isolation. Two horizontal lines were added to the grounded branches to increase the impedance of the proposed antenna. To increase the impedance and decrease MC of the two port antenna in 29 order to adjust the length and positioning of the grounded branches, two horizontal lines were added to the grounded branches. The addition of a T-shaped parasitic element between the two monopole antennas significantly improved isolation. In order to achieve a better isolation and reflection coefficient, the proposed antenna's final structure, which includes four rectangular slots, is reflected in 54.25X36.2X1.524 mm3. The dimensions of the small rectangular cut are etched on the ground plane patch. alterations were made in order to achieve the lowest S21 between the antennas when transmitting and receiving on the same frequency within the FR1 band. To do this, the cut's size was modified. One can achieve a decoupling of -15 dB.

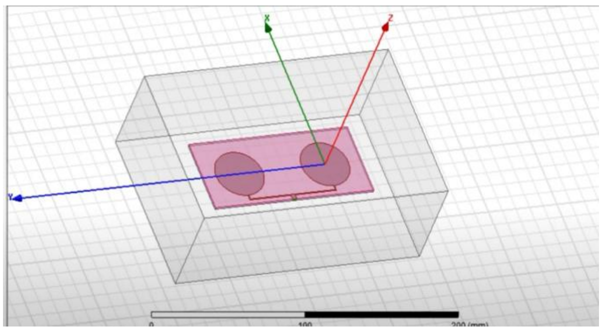

Fig.2.3. 3D View of Dual-Port Circular Patch MIMO Antenna within Radiation Boundary

3. RESULTS AND COMPARATIVE ANALYSIS

A. Scattering parameter

It depicts the simulated (reflection coefficient in dB characteristic of the two port monopole antennas. It observed that the PA has a -10 dB impedance bandwidth (IBW) of 370 MegaHertz (3.3–3.75 GHz.) and achieves good impedance matching and isolation between monopole antennas at resonance frequency with s11, s22, and s21, s12 as <-30 dB and <-15 dB, respectively. The proposed antenna is small in size and has a single passband for 5G new radio sub-6GHz n78band applications.

B. Envelope Correlation Coefficient(ECC), diversity Gain (DG), Total Affective Reflection coefficient(TARC) and VSWR

ECC is used to show how the radiating elements interact and correlate with one another, which is based on the radiation pattern or s-parameters. According to [10] [5], the ECC is obtained from the s-parameter. The achieved simulated 0.01 in Fig. 9 is due to the improved scattering parameter, but ECC < 0.05 is a critical value suitable for practical applications in general.

$$ECC = \frac{|s_{11}^{*} s_{12} + s_{21}^{*} s_{22}|^2}{(1 - |s_{11}|^2 - |s_{21}|^2)(1 - |s_{22}|^2 - |s_{12}|^2)} \quad (1)$$

$$ECC \frac{|\int \int_{4_\pi} [E_i(\theta,\phi) * E_j(\theta,\Phi)] d\Omega|^2}{|\int \int_{4_\pi} |E_i(\theta,\phi)^2| d\Omega * \int \int_{4_\pi} |E_j(\theta,\phi)^2| d\Omega} \quad (2)$$

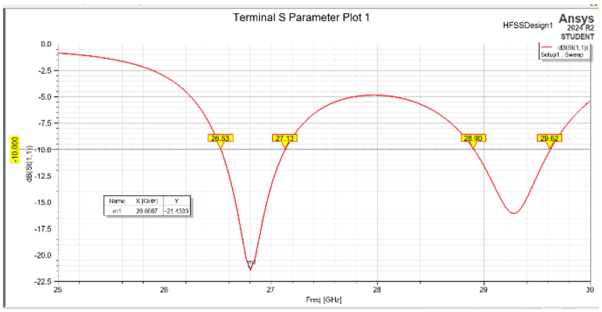

Fig. 3.1. S-Parameter

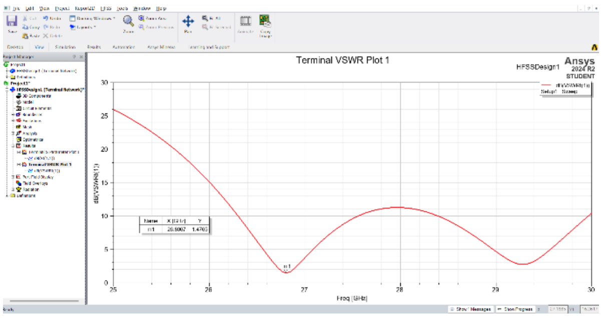

Fig. 3.2. VSWR

The diversity gain is calculated from ECC values; DG [10] [5] graphically depicts simulated values in Fig. 10, and it is nearly 9.99 dB at resonance frequency. The generally accepted value is 10 dB.

$$DG = 10 * \sqrt{(1 - ECC^2)} \quad (3)$$

Fig. 11 demonstrates that the TARC [10] [5]. the response is nearly identical to the individual $|Sii|$ response and achieves -18.22 dB, indicating that the MIMO structure's overall return loss is within an acceptable range, at -15 dB [9] [10].

$$TARC = \sqrt{\frac{|S_{1_1} + S_{1_2}|^2 + |S_{2_1} + S_{2_2}|^2}{2}} \quad (4)$$

VSWR MIMO: More power is transmitted to the antenna and the antenna is better suited to the transmission line when the

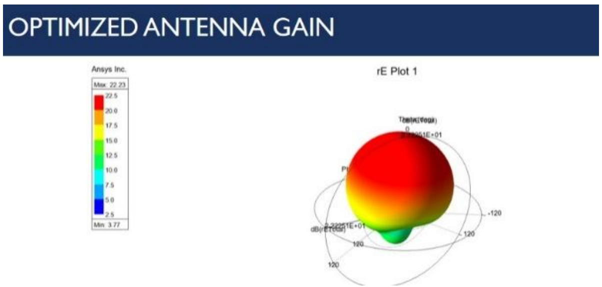

Fig. 3.3. Radiation Plot

VSWR is reduced. VSWR must be at least 1.0. This situation is good because the antenna does not reflect any electricity. Antennas frequently have to meet bandwidth specifications that are expressed in terms of VSWR. For instance, an antenna may advertise VSWR3 operation between 100 and 200 MHz. This suggests that over the chosen frequency range, the VSWR is less than 3.0. Additionally, according to these VSWR standards, the reflection coefficient over the specified frequency range is less than 0.5 (reflection coefficient0.5). VSWR = (1+TARC)/(1-TARC)

4. CONCLUSION

This presents the development and optimization of the proposed MIMO antennas for 5G- NR applications, addressing sub-6 GHz and mm-wave frequency bands. These designs aim to enhance isolation, bandwidth, and efficiency while maintaining a compact size suitable for 5G wireless communication systems. With the increasing demand for compact antennas offering enhanced isolation and diversity, MIMO antenna design has emerged as a critical and fast- evolving research field. The proposed antennas utilize monopole-based MIMO configurations and incorporate various DGS techniques along with DEs such as uniquely shaped stubs to achieve high isolation and superior diversity performance.

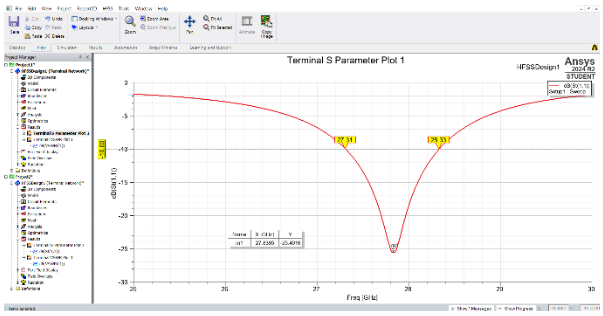

Fig. 3.4. S-Parameter

5 REFERENCES

1.Pandya, K.V. Low Profile Meandered Printed Monopole WiMAX/WLAN Antenna for Laptop, Computer Applications. Micromachines 2022, 13, 2251. https://doi.org/10.3390/mi13122251.

2.Chepala, A.; Fusco, V.; Naeem, U.; McKernan, A. Uniform Linear Antenna Array Beam steering Based on Phase-Locked Loops. Electronics 2023, 12, 780. https://doi.org/10.3390/electronics12040780.

3. Ayaz, M.; Ullah, LA Phased Array Antenna with Novel Composite Right/Left-Handed (CRLH) Phase Shifters for Wi-Fi 6 Communication Systems. Appl. Sci. 2023, 13, 2085. https://doi.org/10.3390/app13042085.

4. Jiménez, D.A.; Reyna, A.; Balderas, L.1.; Panduro, M.A. Design of 4 × 4 Low Profile Antenna Array for CubeSat Applications. Micromachines 2023, 14, 180. https://doi.org/10.3390/mi14010180.

5. Zhao, Y.; Luo, H.; Tan, W.; Zhou, Z.; Zhao, G.; Sun, H. Design of a High-Gain Hybrid Slot Antenna Array Based on Bulk Silicon MEMS Process for W-Band Applications. Electronics 2023, https://doi.org/10.3390/electronics12092028.

6. Daniyal Ali Sehrai, Jalal Khan, Mujeeb Abdullah, Design of high gain base station antenna array for mm-

wave cellular communication systems ,2023, https://doi.org/10.1038/s41598-023-31728.

7. Junli Zhu, Mengfei Chen, Ziting Li, and Jingping Liu, A Compact Planar Ultra-Wideband Array Antenna ,2023, https://doi.org/10.1195/2023/1190236.

8. Yujun Li, Jing Jin, Zhengguang Yang, Low-RCS low-profile MIMO antenna and array antenna using a polarization conversion metasurface ,2023, https://doi.org/10.1364/OE.507087.

9. Yazan Al-Alem, Syed M. Sifa, Millimetre-wave planar antenna array augmented with a low-cost 3D printed dielectric polarizer for sensing and internet of things (IoT), applications, 2023, doi: 10.1038/s41598-023-35707-2.

10. Mohammad Alibakhshikenari, Bal Virdee, Virtual antenna array for reduced energy per bit transmission at Sub-5 GHz mobile wireless communication systems 2023, http://doi.org/10.10163 2023.03.156.

11. Aleksei Dubok and A. Bart Smolders, Senior Member, Focal-Plane Arrays with Improved Scan Capabilities, 2023, IEEE, DOI: 10.1109/TAP 2022.3218931.

12. Amany A Megahed*, Ehab H. Abdelhay, 5G millimeter wave wideband MIMO antenna arrays with high isolation, 2023, https://doi.org/10.1186/513638-023 02267.

13. Pushpa B.R, Pushpa P.V, Design and Simulation of Conformal Array Antennas for Avionics Applications, 2023, doi:10.14445/23488379/IJEEE-V10I9P116.

14. Zhiyun Zhang Yulong Zhou; Tong L, Low-profile shared-aperture metasurface array antenna with ultra-wideband radar cross section reduction and circularly polarization, 2023 https://doi.org/10.1063/5.0163625.

15. Lauri Mela, Alp Karakoc, Low-cost thin film patch antennas and antenna arrays with various background wall materials for indoor wireless communications 2023, doi: 10.1088/2058-8585/accd05.

16. P. Castillo-Tapia et al., "Two-dimensional beam steering using a stacked modulated geodesic Luneburg lens array antenna for 5G and beyond", IEEE Trans. Antennas Propag., vol. 71, no. 1, pp. 487-496, Jan. 2023.

17. Swapna SD, Karthikeya GSD, A High Gain Multi-Port Series Fed Array Realized with Micromachined Low-Cost 3D-Printed Substrate, 2023 https://doi.org/10.1080/02564602.2023.2242828.

18. Kannan Pauliah Nadar, Vanitha Jeyaprakasam, Design and Analysis of Microstrip Patch Antenna Array and Electronic Beam Steering Linear Phased Antenna Array with High Directivity for Space Applications, 2023 https://doi.org/10.1021/acsomega.3c06691.

19. Ali Abdulateef Abdulbari, Sharul Kamal Abdul Rahim, Tan KIM GEOK, et al. Compact 4 x 4 Butler matrix design-based switch beamforming antenna array for 5G applications. Authorea. 2023, doi:10.22541/au.168310020.08218751.